No-Reference Quality Assessment for Multiply-Distorted Images in Gradient Domain

Qiaohong Li, Weisi Lin, *Fellow, IEEE*, and Yuming Fang

***Abstract*—In practice, images available to consumers usually undergo several stages of processing including acquisition, compression, transmission, and presentation, and each stage may introduce certain type of distortion. It is common that images are simultaneously distorted by multiple types of distortions. Most existing objective image quality assessment (IQA) methods have been designed to estimate perceived quality of images corrupted by a single image processing stage. In this letter, we propose a no-reference (NR) IQA method to predict the visual quality of multiply-distorted images based on structural degradation. In the proposed method, a novel structural feature is extracted as the gradient-weighted histogram of local binary pattern (LBP) calculated on the gradient map (GWH-GLBP), which is effective to describe the complex degradation pattern introduced by multiple distortions. Extensive experiments conducted on two public multiply-distorted image databases have demonstrated that the proposed GWH-GLBP metric compares favorably with existing full-reference and NR IQA methods in terms of high accordance with human subjective ratings.**

***Index Terms*—Human visual system (HVS), image quality assessment (IQA), local binary pattern (LBP), multiple distortions, no-reference (NR), structural distortion.**

I. Introduction

THE explosive surge of digital visual signals due to various devices such as digital cameras, web cameras, and smart phones presents challenges on how to store, share, assess, and organize digital images. Since various distortions can be introduced in an image communication system, the received images may be disappointing regarding perceptual quality. Different types of artifacts might be introduced during different processes (acquisition, JPEG compression, JPEG 2000 compression, transmission, etc.) [1]. For example, the defocus scenarios in digital cameras mostly introduce defocus blur artifacts. The inadequacy of capture devices or unfriendly environmental conditions might also induce contrast distortion. The discrete cosine transform (DCT)-based coding techniques mostly bring about blockiness and blur artifacts. The JPEG 2000 standard, which is based on wavelet transform, mostly leads to blur and ringing artifacts. Based on the understanding of these distortions, objective image quality assessment (IQA) methods have been proposed to estimate the perceived image quality through a quantitative approach [2]–[6].

Currently, most IQA studies focus on predicting the visual quality of images distorted by a single distortion. In practice, images available to end users usually undergo several stages, and each stage might introduce certain specific distortion. It is very likely that images are simultaneously distorted by multiple distortions. Compared with visual quality assessment for images with a single type of distortion, it is more difficult for visual quality assessment for multiply-distorted images. Reference [7] pointed out that images with multiple distortions are a big challenge for IQA research and summarized the challenges in three aspects: the influence of individual distortions on image quality, the interaction between these distortions, and the joint effects of these distortions on the overall quality. The author also pointed out that a physical combination of individual distortion measures may not well explain the final overall quality. The two newly established subjective databases on multiply-distorted images, MLIVE (LIVE multiply distorted image quality database) [2] and MDID2013 [8], challenge most existing objective IQA methods and confirm Chandler's statement. Thus, it is much desired to design visual quality methods for images distorted by multiple types of distortions.

Recently, there are several studies focusing on designing objective IQA methods for multiply-distorted images. The authors of [9] proposed an objective no-reference (NR) IQA method based on several image processing blocks to mimic the human visual system (HVS)'s quality assessment process. Specifically, the noise strength is first estimated, followed by blur and JPEG metrics deployed on the denoised image. Then the overall quality is computed by combining the estimated results of noise, blur, and JPEG metrics. This work was later extended by adding a free energy term to account for the possible interaction of different distortions [8]. In [10], natural scene statistics (NSS) features from three existing NR-IQA methods are combined to form an improved bag-of-words representation for quality prediction. Despite the progress in this research area, there are still some problems with these existing methods. These hybrid methods based on the combination of several existing IQA metrics would induce more computational overhead. Furthermore, these methods are tailored for the distortion types in the databases, and the generality to other kinds of multiple distortions is open to question.

In this letter, we propose a novel metric for quality assessment of images containing multiple distortions, without prior knowledge of distortion combination in an image. It has lower computational complexity and higher generality than existing hybrid methods. The new method is based on the HVS's

Manuscript received December 22, 2015; revised February 10, 2016; accepted February 26, 2016. Date of publication March 02, 2016; date of current version March 22, 2016. This work was supported by the Ph.D. Grant from the Institute for Media Innovation, Nanyang Technological University, Singapore; the NSFC under Grant 61571212; and the NSF of Jiangxi Province under Grant 20151BDH80003. The associate editor coordinating the review of this manuscript and approving it for publication was Dr. Guy Gilboa.

Q. Li and W. Lin are with the School of Computer Engineering, Nanyang Technological University, 639798 Singapore (e-mail: qli013@e.ntu.edu.sg; wslin@ntu.edu.sg).

Y. Fang is with the School of Information Technology, Jiangxi University of Finance and Economics, Nanchang, 330013 China (e-mail: fa0001ng@e.ntu.edu.sg).

Color versions of one or more of the figures in this letter are available online at http://ieeexplore.ieee.org.

Digital Object Identifier 10.1109/LSP.2016.2537321

sensitivity to structural degradation. Existing studies show that image structures carry the essential visual information of a scene, and the HVS adaptably extracts structural information for image perception and understanding [11]. Thus, proper extraction and description of image structural information play a significant role in perceptual quality assessment [12]. Here, we propose a novel effective structural feature extraction method as the gradient-weighted histogram of local binary pattern (LBP) calculated on the gradient map (GWH-GLBP). First, the distorted image is filtered by Prewitt operator to extract the gradient. Then LBP is utilized to encode the image primitive microstructures, such as edges, lines, spots, and other local features in the gradient image to form the GLBP. After that, instead of adopting the widely used frequency histogram (FH) to describe the image global structural information, we propose to accumulate the gradient magnitudes of pixels with the same GLBP pattern, which can be regarded as the gradient-weighted GLBP histogram. Finally, support vector regression (SVR) is used to map extracted perceptual features to image quality. Experimental results show that the proposed GWH-GLBP method can deliver superior performance than state-of-the-art methods.

II. Proposed Method

A. GLBP Construction

The gradient magnitudes of digital images are defined as the square root of image directional derivatives along two orthogonal directions. In this work, we adopt the Prewitt filters to compute image gradients due to its computational simplicity. The gradient magnitudes of a distorted image are computed by convolving images with Prewitt filters as follows:

$$\mathbf{g}(i) = \sqrt{(\mathbf{d} * \mathbf{p}_x)^2(i) + (\mathbf{d} * \mathbf{p}_y)^2(i)} \tag{1}$$

where symbol "*" denotes the convolution operation; $\mathbf{p}_x$ and $\mathbf{p}_y$ are the Prewitt filters; $\mathbf{d}$ and $\mathbf{g}$ denote the distorted image and its corresponding gradient magnitude map with i as the location index.

After that, we calculate the LBP for each pixel in the gradient magnitude map. The LBP operator [13] is proposed to describe the relationship between the center pixel and its surrounding neighbors by computing gray-level differences. By applying the LBP operator on the gradient magnitude map, the GLBP code at one location is deduced as

$$\mathrm{GLBP}_{P,R} = \sum_{i=0}^{P-1} s(g_i - g_c)2^i \tag{2}$$

where P is the number of neighbors and R is the radius of the neighborhood. g_c and g_i are the gradient magnitudes at the center location and its neighbor.

The thresholding function $s(\cdot)$ is defined as

$$s(g_i - g_c) = \begin{cases} 1, & g_i - g_c \geq 0 \\ 0, & g_i - g_c < 0. \end{cases} \tag{3}$$

To achieve rotation invariance, a locally rotation invariant uniform GLBP operator can be defined as

$$\mathrm{GLBP}^{\mathrm{riu2}}_{P,R} = \begin{cases} \sum_{i=0}^{P-1} s(g_i - g_c), & \text{if } \mathcal{U}(\mathrm{GLBP}_{P,R}) \leq 2 \\ P+1, & \text{else} \end{cases} \tag{4}$$

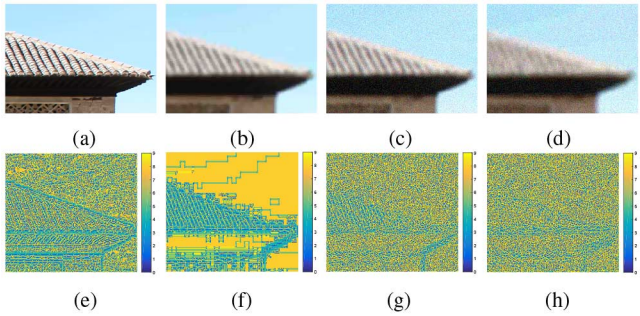

Fig. 1. GLBP maps under different multiple distortions. (a) Pristine image. (b) Image with GB+JPEG. (c) Image with GB+WN. (d) Image with GB+JPEG+WN. (e)–(h) Corresponding GLBP maps of images in the first row.

where $\mathcal{U}$ is the uniform measure, and superscript riu2 denotes the rotation invariant "uniform" patterns with $\mathcal{U}$ value less than 2. The uniformity measure $\mathcal{U}$ is calculated as the number of bitwise transitions

$$\mathcal{U}(\mathrm{GLBP}_{P,R}) = \|s(g_{P-1} - g_c) - s(g_0 - g_c)\| + \sum_{i=0}^{P-1} \|s(g_i - g_c) - s(g_{i-1} - g_c)\|. \tag{5}$$

It was observed that uniform LBP, which contains at most two spatial bitwise transitions, increases the discriminative abilities of LBP [13]. The rotation invariant uniform GLBP would have $P + 2$ patterns, which describe the distinct local gradient structures.

GLBP describes the interpixel relationship in an image neighborhood, and such image microstructural patterns are effective to capture the complex degradation by various distortions. Different GLBP patterns denote different local gradient patterns. For example, in the case of $\mathrm{GLBP}_{8,1}$, (0) stands for isolated gradient spot; (8) denotes smooth region, and (1–7) represents edges of varying positive and negative curvatures. The introduction of distortions may shift the GLBP pattern from one type to another. The first row of Fig. 1 shows one pristine image patch and its three distorted versions; while the second row shows their corresponding GLBP maps. As can be seen in Fig. 1, different distortions change the GLBP patterns in their own characteristic ways, making it an effective measure to describe the impact of various distortions.

B. Gradient-Weighted GLBP Histogram

GLBP is derived from the difference between center pixel and its neighbors in the gradient magnitude map, and thus, it is invariant to the center pixel value (i.e., gradient magnitude at that location). Furthermore, GLBP only encodes the sign of the difference to represent local pattern and excludes the magnitude of the difference; this mechanism makes GLBP unable to differentiate a weak contrast local pattern from a strong one. However, local contrast change has a significant impact on the perception of image quality. Image gradient magnitude is an effective measure to encode contrast information and the HVS is highly sensitive to it. To effectively capture the contrast and structural information in an image, we propose to fuse the structural and gradient information into a single representation. Specifically, we propose to accumulate the gradient magnitudes

of pixels with the same GLBP pattern, which can be regarded as the gradient-weighted GLBP histogram

$$h_{glbp}(k) = \sum_{i=1}^{N} \omega_i f(\mathrm{GLBP}_{P,R}(i), k) \tag{6}$$

$$f(x,y) = \begin{cases} 1, & x = y \\ 0, & \text{otherwise} \end{cases} \tag{7}$$

where N denotes the number of image pixels, $k \in [0, K]$ is the possible GLBP patterns, and ω_i is the weight assigned to the GLBP code. In this work, we use the gradient magnitude calculated by (1) as the GLBP weight of each pixel. In such a way, we emphasize image regions with high contrast changes and take into account the structural and contrast information in a single representation. For the traditional FH, ω_i at each location is the same.

The principle of global precedence has revealed that the HVS perceives image edges in a coarse-to-fine strategy [14]. Thus, the proposed features are extracted at multiscale. Besides the original image scale, the coarser scale is formed by low-pass filtering and downsampling by a factor of 2 in each dimension. During implementation, for GLBP calculation, the number of neighbors P is 8, and the radius of the neighborhood R is 1. The proposed structural features are extracted at five scales. Thus, the extracted features are 50 dimensions in total. The MATLAB source code and validation results are publicly online at http://www.ntu.edu.sg/home/wslin/Publications.htm.

The SVR with radial basis function (RBF) kernel is adopted as the mapping function for feature pooling from the feature space to quality measure [15].

III. Experimental Results and Discussions

A. Databases and Evaluation Methodology

The comparison experiments were conducted on two multiply-distorted image databases (i.e., MLIVE, MDID2013). The MLIVE database [2] consists of two subsets. The first subset includes 15 reference images distorted by GB+JPEG (Gaussian Blur followed by JPEG compression). The second subset includes the same 15 reference images distorted by GB+WN (Gaussian Blur followed by white noise). There are 450 distorted images in total. The MDID2013 database [8] consists of images successively corrupted by three kinds of distortions (GB+JPEG+WN). There are a total of 324 distorted images generated from 12 reference images.

The IQA metrics are evaluated by three criteria: 1) Spearman rank-order correlation coefficient (SRCC) for prediction monotonicity; 2) Pearson linear correlation coefficient (PLCC); and 3) root-mean-squared error (RMSE) for prediction accuracy. The latter two criteria are calculated after the monotonic logistic mapping [16].

B. Performance Comparison With Full-Reference IQA Methods

In this section, we compare the proposed GWH-GLBP with several state-of-the-art full-reference (FR) IQA methods, including PSNR, NQM [17], SSIM [11], IW-SSIM [18], OSS-SSIM [19], VIF [20], VSNR [21], MAD [22], ADM [23], FSIM [24], GMS [25], IGM [26], VSI [27], and GMSD [28].

TABLE I
Performance Comparison With State-of-the-Art FR-IQA Metrics

IQA model	MLIVE (450 images)			MDID2013 (324 images)		
	SRCC	PLCC	RMSE	SRCC	PLCC	RMSE
PSNR	0.728	0.818	10.868	0.643	0.652	0.036
NQM [17]	**0.924**	0.930	6.797	0.715	0.695	0.034
SSIM [11]	0.902	0.926	6.969	0.622	0.656	0.037
IW-SSIM [18]	0.911	0.931	**6.626**	0.890	0.890	0.022
OSS-SSIM [19]	0.919	0.931	6.681	0.763	0.729	0.033
VIF [20]	0.915	**0.932**	6.761	**0.905**	**0.915**	**0.020**
VSNR [21]	0.828	0.880	8.881	0.636	0.652	0.037
MAD [22]	0.894	0.914	7.608	0.856	0.860	0.025
ADM [23]	0.909	0.924	7.051	0.830	0.848	0.026
FSIM [24]	0.895	0.917	7.307	0.749	0.770	0.031
GMS [25]	0.887	0.913	7.429	0.785	0.804	0.029
IGM [26]	0.889	0.923	7.195	0.878	0.882	0.022
VSI [27]	0.877	0.910	7.658	0.730	0.744	0.032
GMSD [28]	0.880	0.911	7.656	0.877	0.902	0.021
GWH-GLBP	**0.944**	**0.949**	**5.873**	**0.908**	**0.913**	**0.019**

The best two IQA metrics are highlighted in boldface.

Since GWH-GLBP adopts SVR learning for quality estimation, the database needs to be divided into training and testing sets. In the experiments, for each database, distorted images of 80% of the reference images are used for training, and the rest are used for testing. This random training–testing split is repeated 1000 times, and the median performance is reported. We also report the median performance across 1000 trials of FR-IQA methods on the testing set for consistent comparison. The prediction performance on the two databases measured by SRCC, PLCC, and RMSE criteria is listed in Table I.

From Table I, we can draw the following conclusions.

1) The best two FR-IQA methods on MLIVE database are NQM and VIF. NQM models the degradation process as linear frequency attenuation followed by additive Gaussian noise [17]. VIF quantifies the information loss between reference and distorted image as quality score [20]. These two methods can well approximate the distortion combinations in MLIVE database and thus deliver better performance than other metrics.
2) The best two FR-IQA methods on MDID2013 database are VIF and IW-SSIM. We attribute the good performance of VIF and IW-SSIM to the decent NSS model [Gaussian scale mixtures (GSM) model in wavelet domain] and the information fidelity philosophy [20].
3) The performance of all methods on MDID2013 is inferior to their performance on MLIVE database. This seems intuitive since degradation in MLIVE is formed by combining two individual distortion types and the degradation in MDID2013 is formed by combining three individual distortion types. The more complex scenario makes the IQA task even more challenging.
4) The proposed NR method GWH-GLBP outperforms all competing FR-IQA methods on MLIVE database. On MDID2013 database, it delivers similar performance with VIF and outperforms all other FR methods.

C. Performance Comparison With NR-IQA Methods

In this section, we compare the proposed GWH-GLBP with several state-of-the-art NR-IQA methods, including BIQI [31], BLIINDS2 [32], DIIVINE [33], CORNIA [34], BRISQUE

TABLE II
PERFORMANCE AND RUN-TIME COMPARISON OF NR-IQA METRICS

IQA model	Time cost (s)	MLIVE (450 images)						MDID2013 (324 images)			
		SRCC	STD	PLCC	RMSE	DT1	DT2	SRCC	STD	PLCC	RMSE
NIQE [29]	0.227	0.789*	0.062	0.858	9.489	0.894	0.832	0.614*	0.105	0.645	0.037
ILNIQE [30]	9.840	0.900*	0.039	0.914	7.538	0.910	**0.916**	0.707*	0.208	0.709	0.034
BIQI [31]	0.050	0.883*	0.052	0.905	7.833	0.881	0.883	0.863*	0.156	0.883	0.023
BLIINDS2 [32]	61.393	0.887*	0.052	0.904	7.981	0.898	0.892	0.808*	0.118	0.844	0.027
DIIVINE [33]	15.519	0.866*	0.059	0.898	8.257	0.865	0.881	0.836*	0.081	0.848	0.026
CORNIA [34]	2.449	0.900*	**0.038**	0.916	7.586	0.905	0.903	**0.898***	**0.077**	**0.904**	**0.020**
BRISQUE [35]	0.079	0.900*	0.052	0.924	7.143	0.907	0.904	0.819*	0.110	0.833	0.027
GMLOG [36]	0.063	0.833*	0.059	0.872	9.164	0.867	0.819	0.824*	0.120	0.830	0.027
NFERM [37]	54.225	0.898*	0.044	0.917	7.459	**0.918**	0.887	0.855*	0.093	0.871	0.024
SISBLM [8]	3.336	**0.907***	0.057	**0.925**	**7.194**	0.908	0.913	0.885*	0.091	0.885	0.023
GWH-GLBP	0.105	**0.944**	**0.029**	**0.949**	**5.873**	**0.936**	**0.953**	**0.908**	**0.076**	**0.913**	**0.019**

The best two IQA metrics are highlighted in boldface.

[35], GMLOG [36], NFERM [37], NIQE [29], ILNIQE [30], and SISBLM [8].

The source codes of the compared NR-IQA methods are obtained from their original authors. The same 80%–20% database split and 1000 times cross validation as in Section III-B are employed here. We have also optimized the SVR parameters of these models to achieve their best performance for fair comparison.

The performance comparison of NR-IQA methods is listed in Table II. To show the robustness of NR-IQA models to the variation in training set, we report the standard deviation (STD) of SRCC values across 1000 trails. The smaller the STD is, the more stable the model to variation in training data. We also report the SRCC on two individual distortion types (DT1 and DT2) on MLIVE database in this table. From Table II, we can draw the following conclusions.

1) The best two NR-IQA methods on MLIVE database are GWH-GLBP and SISBLM. ILNIQE, BRISQUE, and CORNIA are with the third place.
2) The best three NR-IQA methods on MLIVE database are GWH-GLBP, CORNIA, and SISBLM.
3) The performance of all NR methods on MDID2013 is inferior to their counterpart on MLIVE database.

Among them, GWH-GLBP and SISBLM are specifically designed to assess multiply-distorted images, while other methods are general purpose NR-IQA methods.

To further prove the superiority of the proposed method over competing NR-IQA methods, we calculated the statistical significance by two sample T-test between SRCC obtained by competing NR-IQA methods. The results are shown in Table II, where the symbol "*" means that the proposed method is statistically (with 95% confidence) better than the corresponding NR-IQA approach. From Table II, we can see that GWH-GLBP performs significantly better than all other NR-IQA methods on the two databases.

Furthermore, the feature extraction time consumed by each NR-IQA method for estimating the quality of one 512×512 image is also listed in Table II (the second column). Experiments were performed on a ThinkPad T430S notebook with Intel Core i7-3520M CPU at 2.9 GHz. We can see that the proposed method is also computationally efficient.

D. Discussions

From the experimental results, we can see that the proposed method can obtain promising performance in visual quality prediction. The performance improvement is mainly from two aspects. First, the performance of LBP for IQA is improved by Prewitt operator prior to feature extraction. As LBP describes the circular binary first-order derivatives at a microlevel, Prewitt operator is used to enhance the gradient information accordingly. Second, since human visual cortex is sensitive to contrast change and the gradient magnitude measures the contrast information at each location, it is important to emphasize edge information for the integration from local feature to global one. The gradient-weighted GLBP histogram which combines the contrast and structural information can provide better representation for IQA tasks. Here, we examine these two above aspects through experimental comparison.

TABLE III
SRCC COMPARISON FOR DIFFERENT METHODS

Feature	MLIVE	MDID2013
LBP + FH	0.914	0.834
GLBP + FH	0.929	0.870
GWH-GLBP	0.944	0.908

In Table III, the first row "LBP + FH" refers to the feature extraction method that applies the LBP in the original grayscale image, and uses the corresponding FH as the image global feature. The second row "GLBP + FH" refers to the method that applies the LBP in the gradient image, and uses the corresponding FH as the image global feature. From Table III, we observed that both GLBP and gradient-weighting strategy improve the performance in quality prediction.

IV. CONCLUSION

In this study, we have proposed an NR-IQA model named GWH-GLBP to estimate the visual quality of multiply-distorted images based on structural degradation. Specifically, a novel effective structural feature, the GWH-GLBP, is used to characterize image structural information for visual quality estimation. The proposed GWH-GLBP has been compared comprehensively with fourteen representative FR-IQA methods and ten prominent NR-IQA methods on two public multidistortion databases. Experimental results demonstrate the outstanding performance in terms of both prediction accuracy and computational efficiency, making GWH-GLBP a good candidate to be used in practical applications.

REFERENCES

[1] W. Lin and C.-C. J. Kuo, "Perceptual visual quality metrics: A survey," *J. Visual Commun. Image Represent.*, vol. 22, no. 4, pp. 297–312, 2011.

[2] D. Jayaraman, A. Mittal, A. Moorthy, and A. Bovik, "Objective quality assessment of multiply distorted images," in *Proc. Conf. Rec. 46th Asilomar Conf. Signals Syst. Comput. (ASILOMAR)*, Nov. 2012, pp. 1693–1697.

[3] Z. Wang, H. R. Sheikh, and A. C. Bovik, "No-reference perceptual quality assessment of JPEG compressed images," in *Proc. IEEE Int. Conf. Image Process. (ICIP)*, 2002, vol. 1, pp. I–477.

[4] P. Marziliano, F. Dufaux, S. Winkler, and T. Ebrahimi, "Perceptual blur and ringing metrics: Application to JPEG2000," *Signal Process.: Image Commun.*, vol. 19, no. 2, pp. 163–172, 2004.

[5] Y. Fang, K. Ma, Z. Wang, W. Lin, Z. Fang, and G. Zhai, "No-reference quality assessment of contrast-distorted images based on natural scene statistics," *IEEE Signal Process. Lett.*, vol. 22, no. 7, pp. 838–842, Jul. 2015.

[6] K. Gu, G. Zhai, W. Lin, and M. Liu, "The analysis of image contrast: From quality assessment to automatic enhancement," *IEEE Trans. Cybern.*, vol. 46, no. 1, pp. 284–297, Jan. 2016.

[7] D. M. Chandler, "Seven challenges in image quality assessment: Past, present, and future research," *ISRN Signal Process.*, vol. 2013, p. 53, 2013, doi: 10.1155/2013/905685.

[8] K. Gu, G. Zhai, X. Yang, and W. Zhang, "Hybrid no-reference quality metric for singly and multiply distorted images," *IEEE Trans. Broadcast.*, vol. 60, no. 3, pp. 555–567, Sep. 2014.

[9] K. Gu *et al.*, "FISBLIM: A five-step blind metric for quality assessment of multiply distorted images," in *Proc. IEEE Workshop Signal Process. Syst. (SiPS)*, Oct. 2013, pp. 241–246, doi: 10.1117/12.655442.

[10] Y. Lu, F. Xie, T. Liu, Z. Jiang, and D. Tao, "No reference quality assessment for multiply-distorted images based on an improved bag-of-words model," *IEEE Signal Process. Lett.*, vol. 22, no. 10, pp. 1811–1815, Oct. 2015.

[11] Z. Wang, A. C. Bovik, H. R. Sheikh, and E. P. Simoncelli, "Image quality assessment: From error visibility to structural similarity," *IEEE Trans. Image Process.*, vol. 13, no. 4, pp. 600–612, 2004.

[12] J. Wu, W. Lin, G. Shi, and L. Xu, "Reduced-reference image quality assessment with local binary structural pattern," in *Proc. IEEE Int. Symp. Circuits Syst. (ISCAS)*, Jun. 2014, pp. 898–901.

[13] T. Ojala, M. Pietikäinen, and T. Mäenpää, "Multiresolution gray-scale and rotation invariant texture classification with local binary patterns," *IEEE Trans. Pattern Anal. Mach. Intell.*, vol. 24, no. 7, pp. 971–987, Jul. 2002.

[14] H. C. Hughes, G. Nozawa, and F. Kitterle, "Global precedence, spatial frequency channels, and the statistics of natural images," *J. Cognit. Neurosci.*, vol. 8, no. 3, pp. 197–230, 1996, doi: 10.1162/jocn.1996.8.3.197.

[15] B. Schölkopf and A. J. Smola, *Learning With Kernels: Support Vector Machines, Regularization, Optimization, and Beyond*. Cambridge, MA, USA: MIT Press, 2002.

[16] (Aug 2003). *Final report from the video quality experts group on the validation of objective models of video quality assessment—Phase II* [Online]. Available: http://www.vqeg.org/.

[17] N. Damera-Venkata, T. Kite, W. Geisler, B. Evans, and A. Bovik, "Image quality assessment based on a degradation model," *IEEE Trans. Image Process.*, vol. 9, no. 4, pp. 636–650, Apr. 2000.

[18] Z. Wang and Q. Li, "Information content weighting for perceptual image quality assessment," *IEEE Trans. Image Process.*, vol. 20, no. 5, pp. 1185–1198, May 2011.

[19] K. Gu, M. Liu, G. Zhai, X. Yang, and W. Zhang, "Quality assessment considering viewing distance and image resolution," *IEEE Trans. Broadcast.*, vol. 61, no. 3, pp. 520–531, Sep. 2015.

[20] H. Sheikh and A. Bovik, "Image information and visual quality," *IEEE Trans. Image Process.*, vol. 15, no. 2, pp. 430–444, Feb. 2006.

[21] D. Chandler and S. Hemami, "VSNR: A wavelet-based visual signal-to-noise ratio for natural images," *IEEE Trans. Image Process.*, vol. 16, no. 9, pp. 2284–2298, Sep. 2007.

[22] E. C. Larson and D. M. Chandler, "Most apparent distortion: Full-reference image quality assessment and the role of strategy," *J. Electron. Imag.*, vol. 19, no. 1, pp. 011 006-1–011 006-21, 2010.

[23] S. Li, F. Zhang, L. Ma, and K. N. Ngan, "Image quality assessment by separately evaluating detail losses and additive impairments," *IEEE Trans. Multimedia*, vol. 13, no. 5, pp. 935–949, Oct. 2011.

[24] L. Zhang, D. Zhang, X. Mou, and D. Zhang, "FSIM: A feature similarity index for image quality assessment," *IEEE Trans. Image Process.*, vol. 20, no. 8, pp. 2378–2386, Aug. 2011.

[25] A. Liu, W. Lin, and M. Narwaria, "Image quality assessment based on gradient similarity," *IEEE Trans. Image Process.*, vol. 21, no. 4, pp. 1500–1512, Apr. 2012.

[26] J. Wu, W. Lin, G. Shi, and A. Liu, "Perceptual quality metric with internal generative mechanism," *IEEE Trans. Image Process.*, vol. 22, no. 1, pp. 43–54, Jan. 2013.

[27] L. Zhang, Y. Shen, and H. Li, "VSI: A visual saliency-induced index for perceptual image quality assessment," *IEEE Trans. Image Process.*, vol. 23, no. 10, pp. 4270–4281, Oct. 2014.

[28] W. Xue, L. Zhang, X. Mou, and A. Bovik, "Gradient magnitude similarity deviation: A highly efficient perceptual image quality index," *IEEE Trans. Image Process.*, vol. 23, no. 2, pp. 684–695, Feb. 2014.

[29] A. Mittal, R. Soundararajan, and A. Bovik, "Making a completely blind image quality analyzer," *IEEE Signal Process. Lett.*, vol. 20, no. 3, pp. 209–212, Mar. 2013.

[30] L. Zhang, L. Zhang, and A. Bovik, "A feature-enriched completely blind image quality evaluator," *IEEE Trans. Image Process.*, vol. 24, no. 8, pp. 2579–2591, Aug. 2015.

[31] A. K. Moorthy and A. C. Bovik, "A two-step framework for constructing blind image quality indices," *IEEE Signal Process. Lett.*, vol. 17, no. 5, pp. 513–516, May 2010.

[32] M. A. Saad, A. C. Bovik, and C. Charrier, "Blind image quality assessment: A natural scene statistics approach in the DCT domain," *IEEE Trans. Image Process.*, vol. 21, no. 8, pp. 3339–3352, Aug. 2012.

[33] A. K. Moorthy and A. C. Bovik, "Blind image quality assessment: From natural scene statistics to perceptual quality," *IEEE Trans. Image Process.*, vol. 20, no. 12, pp. 3350–3364, Dec. 2011.

[34] P. Ye, J. Kumar, L. Kang, and D. Doermann, "Unsupervised feature learning framework for no-reference image quality assessment," in *Proc. IEEE Conf. Comput. Vis. Pattern Recognit. (CVPR)*, 2012, pp. 1098–1105.

[35] A. Mittal, A. K. Moorthy, and A. C. Bovik, "No-reference image quality assessment in the spatial domain," *IEEE Trans. Image Process.*, vol. 21, no. 12, pp. 4695–4708, Dec. 2012.

[36] W. Xue, X. Mou, L. Zhang, A. C. Bovik, and X. Feng, "Blind image quality assessment using joint statistics of gradient magnitude and laplacian features," *IEEE Trans. Image Process.*, vol. 23, no. 11, pp. 4850–4862, Nov. 2014.

[37] K. Gu, G. Zhai, X. Yang, and W. Zhang, "Using free energy principle for blind image quality assessment," *IEEE Trans. Multimedia*, vol. 17, no. 1, pp. 50–63, Jan. 2015.